Addressing the Effect of Sloping Terrain on Ground Movements Due to Underground Mining

Z. Agioutantis
Virginia Center for Coal and Energy, Virginia Tech, Blacksburg, Virginia

M. Karmis
Virginia Center for Coal and Energy, Virginia Tech, Blacksburg, Virginia

ABSTRACT

The prediction of ground movements due to underground mining is now a mature methodology that can be applied to perform accurate and realistic predictions of potential impacts to surface structures and facilities. Through the application of the influence function method, a number of deformation indices can be calculated using average or conservative parameters, including subsidence, slope, horizontal strain and surface curvature, at any point on the surface, or at any other elevation above the extracted seam.

In the case of horizontal displacement calculations, research has identified the effect of sloping terrain on the displacement vectors. Surface points, once disturbed by the subsidence process, tend to displace downwards, due to sloping surface terrain, as well as towards the subsidence trough.

In this paper, a new tool will be presented that provides a methodology to allow for site specific adjustments of horizontal displacements due to sloping terrain. This method has been incorporated into the Surface Deformation Prediction System (SDPS) package developed at Virginia Tech. A case study is presented where the application of the terrain slope adjustment in ground movement predictions is validated by field measurements.

INTRODUCTION

It is well documented in the literature (Peng and Luo 1989; Luo et al. 1996) that horizontal displacements induced by underground mining under sloping terrain may be different from horizontal displacements measured on a flat surface. Furthermore, Luo et al. (1996) conclude that the main factors that affect the magnitude and orientation of horizontal displacement of surface points are the total movement at each point and the angle of the natural slope at each point. According to their analysis, total movement includes both vertical and horizontal incremental displacements, prior to applying any corrections due to the sloping terrain. At the same time, work by Khair et al. (1987) indicates that topography has no effect on the amount of vertical subsidence, but "the direction of horizontal displacements exclusively depends on topography when the slope is significantly large."

It is evident that at a particular point, the displacement mechanism relates to soil properties and conditions (Karmis et al., 1990; 1991). At a larger scale, mathematical and/or numerical models as described in slope stability evaluation procedures may be applied in order to obtain an overview of movements. This usually involves precise knowledge of soil and overburden mass properties and elastic/plastic response constants, as well as parameters that describe potential sliding failure such as cohesion and angle of internal friction. In this work, a simple mathematical algorithm relying on a single parameter is derived and implemented that allows for more accurate calculations of horizontal displacement over undermined terrain.

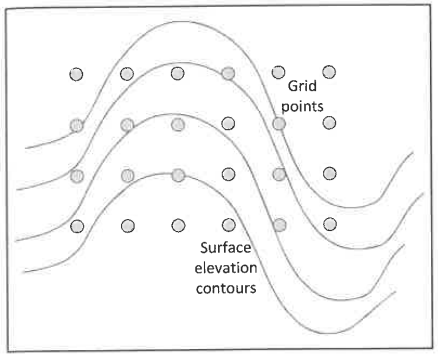

Figure 1. Surface elevation contours and grid points

REPRESENTING SURFACES WITH DIGITAL MODELS

'Digital elevation model' (DEM), 'digital terrain model' (DTM) and 'digital surface model' (DSM) are all terms used to represent a surface terrain (with or without vegetation, structures, etc.) digitally. These models are created from terrain elevation data. Commonly, a DEM can be represented as a vector-based triangular irregular network (TIN) or as a raster (i.e., a set of rectangular grids). In this paper, the term 'digital elevation model' will be used to refer to the digital representation of the topographic surface used in the ground deformation calculations above an undermined area.

In general, more detailed local representations of surfaces are mathematically represented by polynomial equations. Depending on the complexity of such equations, elevation data at several points may be needed to obtain a complete and accurate mathematical model. Elevations at grid points (points on the surface that are evenly spaced as shown in Figure 1. Surface elevation contours and grid points) are commonly used to provide data for such equations.

Although any order of polynomial may be used to model local surface patches, a quadratic function can be regarded as a successful compromise between the number of data points required to uniquely model the surface and the accuracy with which the model fits the true surface. By the nature of such models, it is evident that the equation will be most accurate in the vicinity of these data points. Planar surfaces would only require three points to define the polynomial equation; therefore, they could be modeled using four grid points defining a local window. However, a planar model is rarely sufficient to model actual surfaces in a large or local scale. Polynomials of order three (3) or higher can model more convoluted surfaces including breaks of slope (points of inflection), but require ten points to define the surface. Since this would require a local window of more than 3 by 3 grid points (2 by 2 cells), it is usually impractical for common applications. Thus, the quadratic function, shown in Equation 1, appears the most widely and appropriately used model for general geomorphometric approximation (Wood, 1996). To determine the coefficients of this equation, six known elevation values are needed.

$$z = ax^2 + by^2 + cxy + dx + ey + f \quad (1)$$

Alternatively, Equation 1 can be written in the form of the general conic:

$$ax^2 + by^2 + 2hxy + 2jx + 2ky + m = 0 \quad (2)$$

where $h=c/2$, $j=d/2$, $k=e/2$ 2, and $m=f-z$.

Instances of the general conic fall into one of three types (hyperbolic, parabolic or elliptic), depending on the values of the coefficients a, b and h. Terrain parameters such as slope angle and slope aspect can be defined by considering the partial differential equations of the general quadratic Equation 1 or the general conic Equation 2, as detailed in the following section.

Slope Angle and Slope Aspect

The rate of change of elevation in both the x and y directions can be used to identify the direction and magnitude of the steepest gradient. These two parameters can be found by taking the partial first order derivatives of (1) above, with respect to x and y:

$$\frac{\partial z}{\partial x} = 2ax + cy + d \quad (3)$$

$$\frac{\partial z}{\partial y} = 2by + cx + e \quad (4)$$

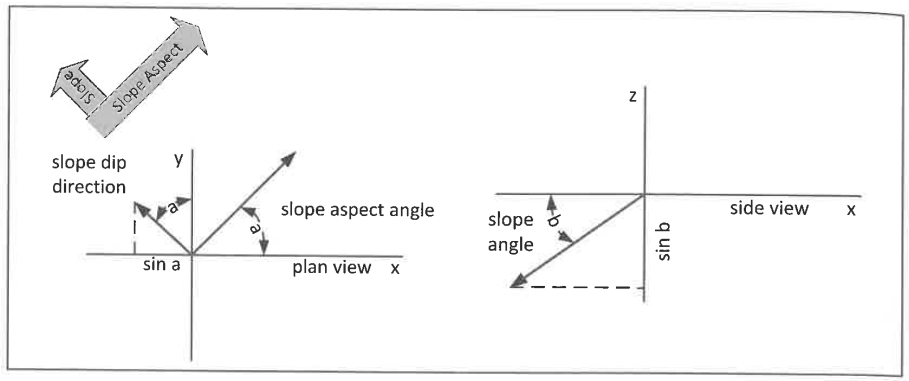

Figure 2. (a) Slope aspect angle and slope dip direction in the x-y axes; (b) slope angle in the x-z axes

The tangent of the maximum slope angle at a point can be found by combining Equations 3 and 4:

$$\text{Slope Tangent} = \sqrt{\left[\frac{\partial z}{\partial x}\right]^2 + \left[\frac{\partial z}{\partial y}\right]^2} \quad (5)$$

By adopting a local coordinate system with the origin located at the point of interest on a specific slope (i.e., x=0, y=0), Equation 5 becomes:

$$\text{Slope Tangent} = \sqrt{d^2 + e^2} \quad (6)$$

where slope is expressed as the tangent of the (maximum) slope angle. Equation 7 shows the conversion of the slope tangent to the slope angle in degrees or radians. The slope angle represents the maximum (natural) slope at the surface location, which is represented by the quadratic Equation 1:

$$\text{Slope Angle} = \arctan\left[\sqrt{d^2 + e^2}\right] \quad (7)$$

In a similar fashion, slope aspect (also known as slope direction or slope bearing) is a line defined by its polar angle, which is described in Equation 9 by the two orthogonal partial derivatives (Srinivasan and Engel, 1991).

$$\text{Slope Aspect} = \arctan\left[\frac{e}{d}\right] \quad (8)$$

The slope dip direction is the actual direction of the maximum slope, and it is always orthogonal to the slope aspect angle. Observing the right-hand coordinate system, the slope dip direction can be calculated by Equation 9:

$$\text{Slope Dip Direction} = \text{Slope Aspect} + 90 \quad (9)$$

Note that Equations 6–9 can also be given in terms of the coefficients of the general conic Equation 2. Figure 2a shows the slope aspect and slope dip direction, while Figure 2b shows the slope angle.

Figure 3 illustrates maximum slope angle and slope direction (aspect) for four cases of planar surfaces digitized by square grids. The numbers in the circles represent elevations in units of length. The dashed lines represent the respective elevation contours, while the arrows show the slope aspect or slope direction and the direction of the maximum slope angle for each case, respectively.

By applying Equations 7 and 8 to the first planar surface, it can be easily calculated that the slope aspect is –45°, the direction of the maximum slope angle is +45°, and the maximum slope angle is about 35°.

CALCULATION OF HORIZONTAL DISPLACEMENTS DUE TO UNDERGROUND MINING USING THE INFLUENCE FUNCTION METHOD

Influence function methods have been widely applied for the calculation of a number of surface deformation indices including subsidence and horizontal displacement. Utilizing the

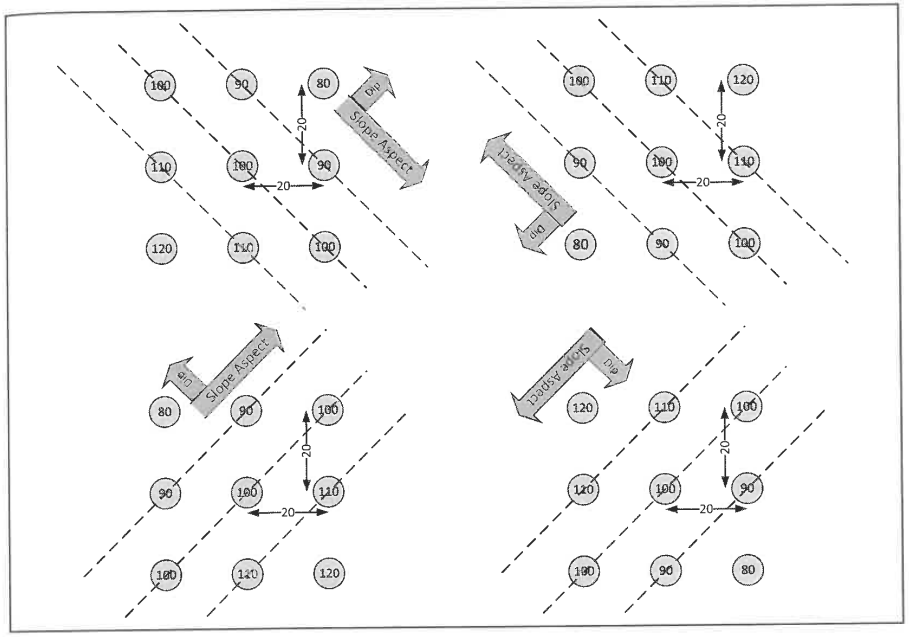

Figure 3. Slope dip direction and slope aspect for four sloping planar surfaces

bell-shaped Gaussian function, subsidence $g(x, s)$ at any point can be given by:

$$g(x,s) = \frac{So(x)}{r} e^{\left(-\pi \frac{(x-s)^2}{r^2}\right)} \quad (10)$$

where

r = the radius of principal influence $= h/\tan(\beta)$;
h = the overburden depth;
β = the angle of principal influence;
s = the coordinate of the point, $P(s)$, where subsidence is considered;
x = the coordinate of the infinitesimal excavated element; and
$So(x)$ = the convergence of the roof of an infinitesimal excavated element

Therefore, subsidence at any point $P(s)$ can be expressed by the following equation:

$$S(x,s) = \frac{1}{r}\int_{-\infty}^{+\infty} So(x)\, e^{\left(-\pi \frac{(x-s)^2}{r^2}\right)} dx$$

and for finite extraction limits (x_1, x_2)

$$S(x,s) = \frac{S\max}{r}\int_{x_1}^{x_2} e^{\left(-\pi \frac{(x-s)^2}{r^2}\right)} dx \quad (11)$$

In the case of the half-infinite horizontal plane excavation, extraction is assumed to occur from x to $+\infty$. By identifying the coordinate s with the coordinate x and by selecting the origin of the coordinate system to be at the edge of the extracted area, Equation 11 can be written as:

$$S(x) = \frac{S\max}{r}\int_{x}^{+\infty} e^{\left(-\pi \frac{\lambda^2}{r^2}\right)} d\lambda \quad (12)$$

Furthermore, Equations 14 and 15 relate the horizontal displacements $U(x)$ and $U(y)$ to the first derivative of subsidence, i.e., tilt for the case a finite size rectangular parcel defined by $(x_1, y_1 - x_2, y_2)$ (see also Karmis et al., 1990):

$$U(x) = -Bs\frac{\partial S(x,y)}{\partial x} = Bs\frac{S\max}{r^2}\left[e^{\left(-\pi\frac{x_2^2}{r^2}\right)} - e^{\left(-\pi\frac{x_1^2}{r^2}\right)}\right] \times \int_{y_1}^{y_2} e^{\left(-\pi\frac{y^2}{r^2}\right)}dy \quad (13)$$

$$U(y) = -Bs\frac{\partial S(x,y)}{\partial y} = Bs\frac{S\max}{r^2}\left[e^{\left(-\pi\frac{y_2^2}{r^2}\right)} - e^{\left(-\pi\frac{y_1^2}{r^2}\right)}\right] \times \int_{x_1}^{x_2} e^{\left(-\pi\frac{x^2}{r^2}\right)}dx \quad (14)$$

here Bs is the strain coefficient in length units.

Using Equations 14 and 15 the horizontal displacement at any surface point (x,y) can be calculated. This calculation depends on the actual location of the surface point, but the point itself is assumed to lie on a horizontal plane at that location.

ADJUSTMENT OF HORIZONTAL DISPLACEMENTS DUE TO SLOPING TERRAIN

As already discussed, the main factors that affect the magnitude and orientation of horizontal displacements at surface points are the total movement at each point (i.e., subsidence and/or horizontal displacement) as well as the direction and angle of the natural slope at each point.

Thus, based on Equations 14 and 15 the adjusted horizontal displacements may be calculated as follows:

$$U'(x) = U(x) + SC * ABS(S(x,y)) * \cos(90 + \text{slope aspect}) * \sin(\text{slope angle}) \quad (15)$$

$$U'(y) = U(y) + SC * ABS(S(x,y)) * \sin(90 + \text{slope aspect}) * \sin(\text{slope angle}) \quad (16)$$

where $S(x,y)$ is the subsidence at point (x,y), SC is a unitless slope coefficient related to the type of top soil and the local conditions.

For the implementation of the above procedure, a detailed digital representation of surface elevations is necessary. If a DEM or a TIN is available, then a detailed grid can be generated and used for calculating the slope aspect and the slope angle.

This methodology has been incorporated into the influence function formulation of the SDPS package to facilitate calculations and visual representation of the results.

DEMONSTRATION EXAMPLE

For this demonstration example, a fully extracted panel of supercritical geometry is defined with the long dimension to the north. A transverse line of monitoring points is defined at mid panel on a planar surface sloping at 10 degrees to the north. A conceptual diagram is given in Figure 4. In order to use the SDPS software, the extraction thickness is set to 5 ft, the percent hardrock to 50%, the tangent of the influence angle (tanb) to 2.31, the strain coefficient (Bs) to 0.35, and the slope coefficient to 0.5. (Note that a slope coefficient of zero is equivalent to no adjustment.)

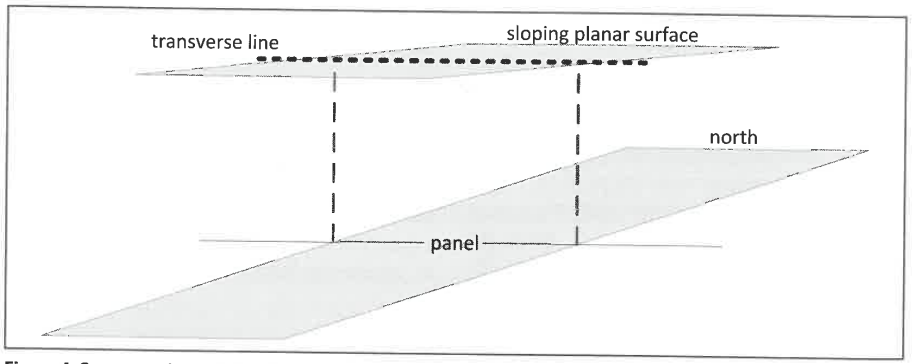

Figure 4. Conceptual diagram of fully extracted panel under a sloping surface

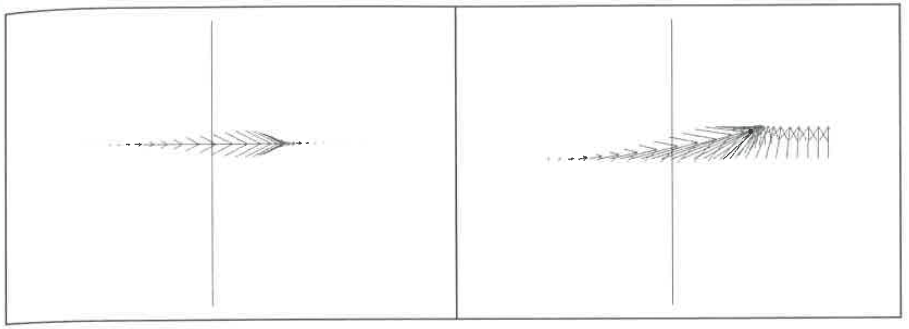

Figure 5. (a) Calculated horizontal displacements without adjustment; (b) calculated horizontal displacements with adjustment; note that only the half panel is shown

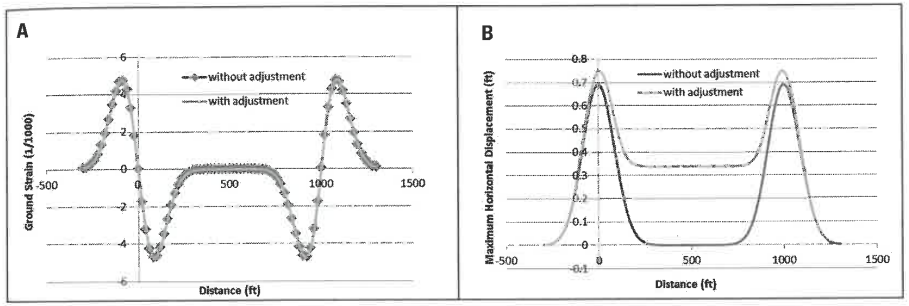

Figure 6. (a) Comparison of ground strains with and without adjustment (the two curves are identical); (b) comparison of horizontal displacement magnitude with and without adjustment

Figure 5 presents the calculated horizontal displacements before and after the adjustment along the monitoring line. As expected, the displacement vectors point downward, towards the foot of the sloping surface. Figure 6a presents the ground strains calculated before and after the adjustment. As expected the change in the strain is negligible. Figure 6b shows the magnitude of the horizontal displacements. It is interesting to note that although the horizontal displacements were zero at the middle of the panel before the adjustment, they assume a positive value after the adjustment. This is to be expected since the sliding mechanism translates these points more than the less-disturbed surface points located at the sides of the trough.

CASE STUDY

The adjustment of horizontal displacements due to sloping terrain using the above methodology is demonstrated for a case of a longwall panel under hilly terrain. Figure 7 shows the layout of the panel, a monitoring line and the surface contours. Overburden depth under the transverse monitoring line to the west of the panel varies from about 350 ft to about 650 ft and seam thickness is about 6.5 ft. Monitoring point spacing is about 100 ft. An edge effect of 150 ft was applied on both sides of the panel. Figure 8 shows the calculated and

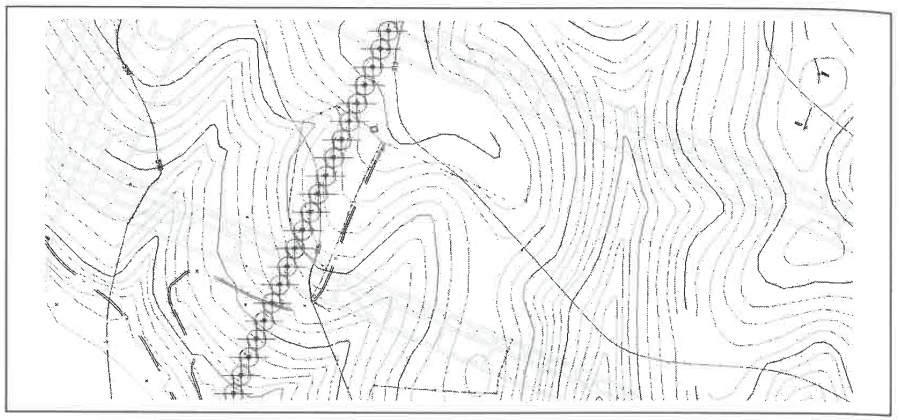

Figure 7. Layout of longwall panel, transverse monitoring line, and surface contours

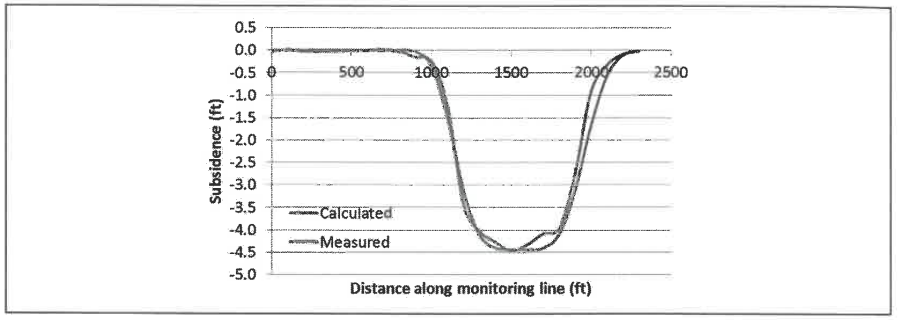

Figure 8. Calculated and measured subsidence along monitoring line

measured subsidence along the monitoring line starting from south going north, assuming full extraction of the panel.

Figure 14 compares the calculated maximum displacement values before and after the adjustment. The horizontal axis represents distance along the monitoring line calculated from the point furthest away from the south west edge of the mine panel. It can be easily observed that the calculated values match very well the measured data for the vertical displacement.

In order to apply the slope adjustment methodology described earlier, a 20×20 ft grid pattern was created based on the surface contour elevations. The spacing of the grid was selected based on the spacing of the available contours, which were set at 20 ft intervals (see Figure 9). The slope aspect and maximum slope were then calculated at the closest grid point to each point on the monitoring line, based on the surface grid shown in Figure 9. The results are shown in Figure 10. Note that the aspect angles are given in a counterclockwise direction from the positive x axis.

Figure 11a presents a plan view of the calculated maximum horizontal displacement vectors over the panel before the adjustment; Figure 11b shows an overlay of the calculated vectors and the measured values. Figure 12 shows a plan view of the adjusted horizontal displacements using Equations 16 and 17 and a slope coefficient equal

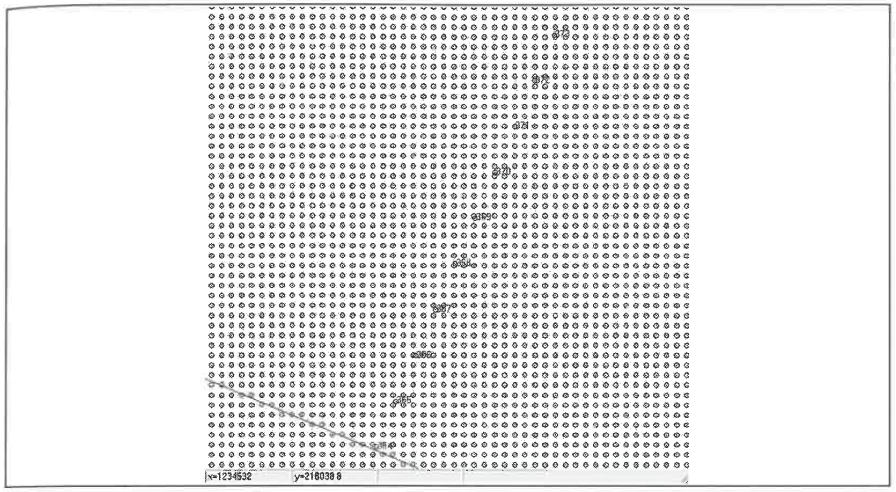

Figure 9. Surface grid points and monitoring points

Point No	Maximum Slope	Slope Aspect
354	13.23	142.44
355	12.69	150.89
356	13.95	152.75
357	17.64	148.34
358	15.17	148.68
359	15.79	145.35
360	14.28	139.19
361	13.05	127.70
362	13.31	122.01
363	14.97	117.81
364	15.50	114.65
365	13.66	110.77
366	12.35	102.03
367	11.23	93.79
368	10.81	87.70
369	12.97	76.77
370	15.20	81.59
371	16.78	96.24
372	11.34	116.94
373	10.58	128.01
374	5.71	259.86
375	4.42	180.98
376	3.55	210.27
377	4.74	342.82

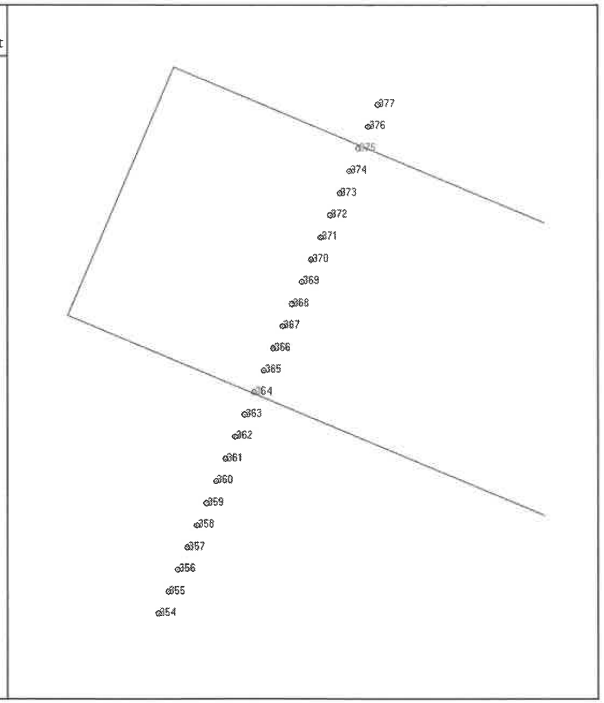

Figure 10. Slope aspect and maximum slope angle calculated for each point on the monitoring line

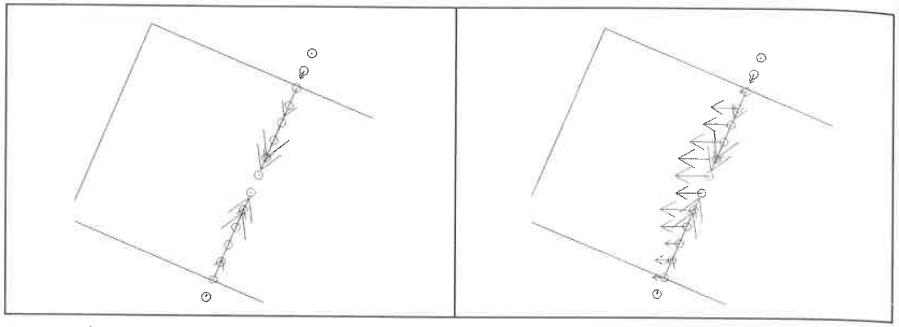

Figure 11. (a) Plot of maximum horizontal displacement vectors without slope adjustment; (b) comparison of horizontal displacement vectors to measured values

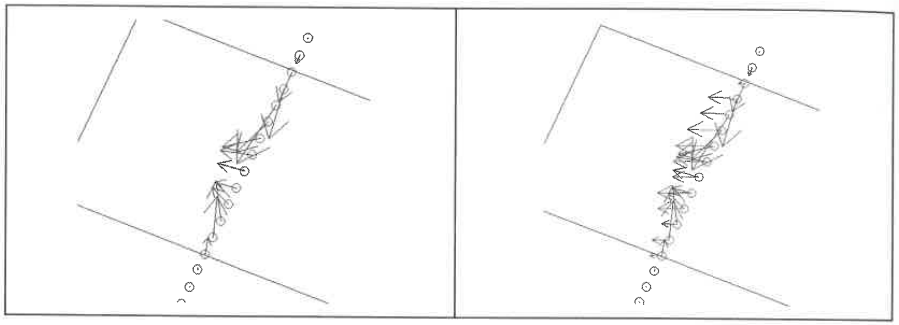

Figure 12. (a) Plot of maximum horizontal displacement vectors with slope adjustment; (b) comparison of horizontal displacement vectors to measured values

to 0.2. Figure 12b presents an overlay of the measured and calculated displacements. It is clear that after applying the adjustment the calculated values follow the natural slope downhill.

Franks and Geddes (1986) suggest that with sloping surfaces the horizontal strain may not be the most useful measure; instead, they propose using the in-plane ground strain as the basic parameter for comparison. Figure 13 compares the calculated ground strain profiles before and after the adjustment. Ground strain is calculated based on directional strain along the monitoring profile adjusted for terrain variation along the same profile. Ground strain is more representative of the strain developed on the ground surface, taking into account the natural terrain and displacements due to the subsidence process. It is evident that the strain profiles before and after the adjustment do not vary significantly as was also demonstrated in the theoretical case.

It can be observed, however, that not all monitoring points follow that trend. This can be attributed to a number of reasons, such as:

- The grid representation of the surface is not as accurate either due to the gridding procedure or due to the original elevation contours. Clearly for this type of calculation a more accurate grid is needed.
- Although the direction of the maximum slope seems to be the major factor, it is possible that other factors contribute to the lateral adjustment of the horizontal displacements calculated at each surface point.

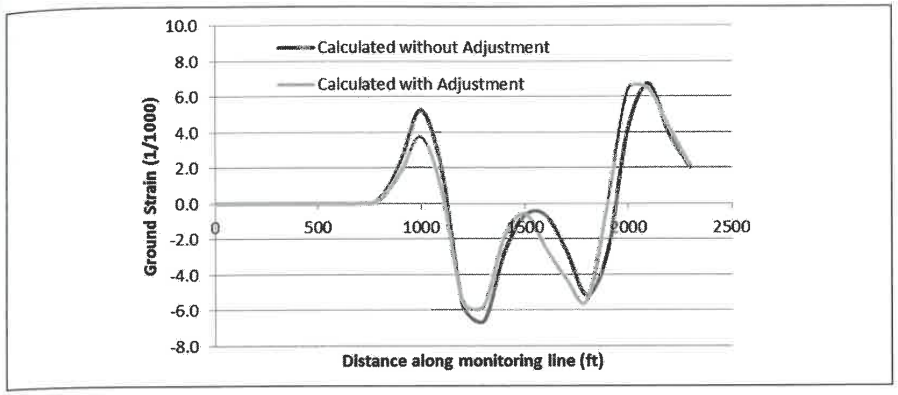

Figure 13. Comparison of calculated ground strain profiles along the monitoring line for displacement vectors with and without adjustment

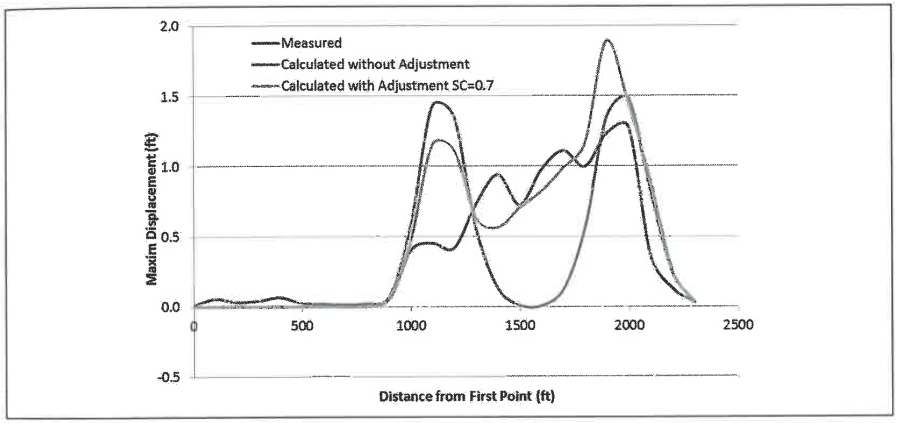

Figure 14. Comparison of maximum horizontal displacement values for measured data, calculated without adjustment and calculated using a slope coefficient SC=0.2

Figure 14 compares the maximum displacement value before and after the adjustment for three cases; measured, calculated without adjustment of the horizontal displacement due to the sloping terrain and calculated after adjusting the horizontal displacements with a slope coefficient equal to 0.7. The horizontal axis represents distance along the monitoring line calculated from the point furthest away from the south west edge of the mine panel.

The high displacement values are calculated in both cases at the high tensile value offsets (Figure 13). However, the adjusted curve matches very well the measured maximum horizontal displacement between the edges of the panel, although the match is not as accurate around the edges of the panel. Results are consistent with the calculations presented for the demonstration example.

CONCLUSIONS

The main factors that affect the magnitude and orientation of horizontal displacements at surface points are the total movement at each point (i.e., subsidence and/or horizontal displacement) as well as the direction and angle of the natural slope at each point. The natural slope conditions at each surface point of interest can be calculated from digital surface models. The simplest such model can be represented by a surface grid generated from surface contours. A quadratic equation is then used for the representation of the natural slope at the cell level.

This paper presents a procedure to adjust the horizontal displacements based on natural slope conditions using a single coefficient. The same correction algorithm is applied to the calculated horizontal displacements of all surface points. The algorithm has been implemented in the Influence Function formation of the SDPS package to facilitate calculations. The algorithm is verified using an actual example of a monitoring line, above a longwall panel, in hilly terrain.

Results of comparing adjusted horizontal displacements to measured data both as vectors on the horizontal plane and as maximum horizontal displacement magnitudes are presented. In both instances the comparison between calculated and adjusted values show that adjusted horizontal displacements using the procedure presented in this paper better match measured values, both in direction and magnitude.

ACKOWLEDGMENT

This study was sponsored by the Appalachian Research Initiative for Environmental Science (ARIES). The views, opinions and recommendations expressed herein are solely those of the authors and do not imply any endorsement by ARIES employees, other ARIES-affiliated researchers or industrial members. Information about ARIES can be found at http://www.energy.vt.edu/ARIES.

REFERENCES

Franks, C.S.M., and Geddes, J.D., 1986, Subsidence on Steep Slopes Due to Longwall Mining, *International Journal of Mining and Geological Engineering*, Vol. 4, No. 4, pp. 291–301.

Karmis, M., Agioutantis Z., and Jarosz, A., 1990, Subsidence Prediction in Steep Slope Terrain. Proceedings, Annual Symposium, Powell River Project, September, pp. 43–55.

Karmis, M., Agioutantis Z., and Jarosz, A., 1991, Subsidence Prediction in Steep Slope Terrain–Model Formulation and Application, Proceedings, Annual Symposium, Powell River Project, September, pp. 46–54.

Karmis, M., Agioutantis Z., and Jarosz, A., 1990, Recent Developments in the Application of the Influence Function Method for Ground Movement Predictions in the U.S., Mining Science and Geotechnology, Vol. 10, pp. 233–245.

Khair, A.W., Quinn, M.K., and Chaffins, R.D., 1987, Effects of Topography on Ground Movement Due to Longwall Mining, Paper presented at SME-AIME annual meeting, Denver, CO, Preprint No. 87–142, 10 p.

Luo, Y., Peng, S.S., and Chen H.J., 1996, Identification of Factors Affecting Horizontal Displacement In Subsidence Process, In *Proceedings 15th International Conference on Ground Control in Mining*, Ed. L. Ozdemir et al., Colorado School of Mines, Golden, CO, pp. 155–165.

Peng, S.S., and Luo, Y., 1989, Slope stability under the influence of ground subsidence due to longwall mining, *Mining Science and Technology*, 8, pp. 89–95.

Srinivasan, R., and Engel, B.A., 1991, Effect of Slope Prediction Methods on Slope and Erosion Estimates. *Applied Engineering in Agriculture*, 7, pp. 779–783.

Wood, J.D., 1996, The geomorphological characterisation of digital elevation models, PhD Thesis, University of Leicester, UK, http://www.soi.city.ac.uk/~jwo/phd.